Manufacturing Considerations in the 3-D Printing of Fractal Antennas

Sung Yun Jun, Benito Sanz-Izquierdo, Edward A. Parker, David Bird, and Alan McClelland

***Abstract*— The use of additive manufacturing (AM) techniques for the fabrication of 3-D fractal monopole antennas is presented. The 3-D printing (3-D P) of 3-D designs based on the Sierpinski fractal concept is studied, and the performance discussed. The AM allows the fabrication of the complex features of these antennas. The specific structures, on the other hand, provide a reduction of the material used in AM compared with the equivalent nonfractal designs, in which two cases can be described by over 75%. This is the first time that 3-D fractals have been studied in terms of volume reduction and their potential benefits to AM of antennas. The first investigated antenna derives from the Sierspinki tetrahedron fractal shape. From this initial design, two new structures have been developed: the dual Sierpinksi fractal and the dual inverse Sierpinski fractal. The new designs offer improved matching and radiation pattern. All the antennas operate at 2.4 GHz used in Bluetooth and wireless LAN band. Furthermore, the final inverse fractal shape is able to cover both the 2.4- and 5.5-GHz WLAN frequencies with a reflection coefficient (S_{11}) better than −10 dB, together with coverage at bands around 8 GHz. This ratio of resonant frequencies is achieved after a series of described design stages. The radiation patterns of the antennas are monopole-like at both bands. The AM technique employed is metal powder embinder printing where a binding material is jetted on a powder bed containing metal particles. Metal 3-D P is ideal for maintaining the mechanical strength of the structures. The envisaged applications are in the defense and aerospace sectors where high-value, lightweight, and mechanically robust antennas can be integrated with other 3-D printed parts. Transient simulations based on the finite integration technique compare well with measurements.**

***Index Terms*— 3-D printing (3-D P) fractal antenna, additive manufacturing (AM), multiband antenna.**

I. Introduction

ADDITIVE manufacturing (AM) or 3-D printing (3-D P) is a technology that is attracting significant attention from the research community and manufacture industry. The 3-D P is able to fabricate complex designs from a digital model. Objects are created layer after layer as opposed to traditional subtractive techniques. The 3-D P is developing very quickly and promises significant advances in the future. Many researchers and industrialists are concentrating their efforts on the development of new techniques and applications in the area of electronics [1], automobiles [2], and medical devices [3]. One area of special interest is in the flexible and rapid prototyping of antenna and microwave components.

A variety of 3-D AM methods have been proposed for the development of microwave devices. This includes fused deposition modeling (FDM) [4], selective laser sintering (SLS) [5] and selective laser melting (SLM) of metallic powders [6], and electron beam melting [7]. In some cases, two different technologies have been combined such as FDM and direct write [8]. In terms of devices, a terahertz dielectric reflectarray was fabricated using SLS and polymer-jetting 3-D P technology in [9], and a microwave lens was fabricated using FDM in [10]. In [11] and [12], fully and partially metalized 3-D frequency selective structures were developed using 3-D P technologies, and in [13], a nonuniform electromagnetic bandgap (EBG) structure was fabricated using FDM.

AM has also been applied to antenna technology [14]–[16]. An electrical meander-line antenna was fabricated on the surface of a conformal hemisphere glass substrate in [14], an electrical small folded spherical helix antenna was 3-D printed and then metalized in [15], and an ultra wideband volcano smoke antenna was fabricated using SLM and then electroplated in [16]. In general, 3-D AM can be a viable solution if the structures contain complex geometrical features and their properties are sufficiently novel or unusual to justify the extra cost involved.

Fractal antennas were introduced more than two decades ago [17], [18]. Since then, they have widely been researched and reported. They offer multiband and multifunctional operations [19], [20] and, in some cases, small physical size. The basic concept of the fractal antenna starts from the iteration of self-similar elements with diverse direction and scale but not changing the main shape. Most of the fractal antennas available in the literature are 2-D, normally based on the monopole [21]–[23] and the patch type [24]. These geometries have been employed in frequency selective surface [25], [26] and EBG structures [27], [28]. More recently, 3-D fractal antennas have been investigated [29], [30]. They provide improved omnidirectional radiation pattern and wider impedance bandwidth.

This paper discusses the fabrication of 3-D fractal antennas using metal AM techniques. The 3-D P allows the fabrication

Manuscript received March 13, 2017; revised June 27, 2017; accepted June 29, 2017. This work was supported in part by the U.K. EPSRC High Value Manufacturing Fellowship under Grant REF: EP/L017121/1, in part by the Royal Academy of Engineering Industrial Secondment Scheme under Grant REF: ISS1617/48, and in part by the Royal Society Research Grant under Grant REF: RG 130637. Recommended for publication by Associate Editor S. Grivet-Talocia upon evaluation of reviewers' comments. *(Corresponding author: Benito Sanz-Izquierdo.)*

S. Y. Jun, B. Sanz-Izquierdo, and E. A. Parker are with the School of Engineering and Digital Arts, University of Kent, Canterbury CT2 7NT, U.K. (e-mail: sj329@kent.ac.uk; b.sanz@kent.ac.uk; e.a.parker@kent.ac.uk).

D. Bird and A. McClelland are with The Centre for Process Innovation, Sedgefield TS21 3FG, U.K. (e-mail: David.Bird@uk-cpi.com; Alan.McClelland@uk-cpi.com).

Color versions of one or more of the figures in this paper are available online at http://ieeexplore.ieee.org.

Digital Object Identifier 10.1109/TCPMT.2017.2730366

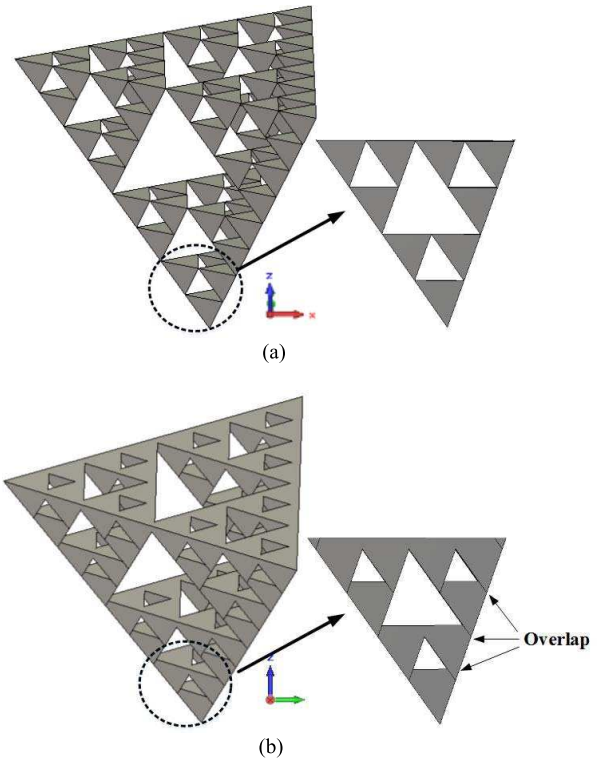

Fig. 1. Perspective view of the Sierpinski fractal antenna. (a) Without overlap. (b) With overlap.

of the complex features of fractal models. The 3-D fractal shapes based on the Sierpinski concept are proposed. These structures have the important property of being able to reduce the amount of material used in an AM process, which can lead to lighter weight devices. This is the first time that 3-D fractals have been discussed in terms of potential material reduction and their benefit to the AM of microwave components. Material volume reduction is achieved in relation to the equivalent tetrahedron-based shapes. Although other types of antenna design, such as planar form structures, may provide better overall volume efficiency, the challenge here has been to use this manufacturing technique to fabricate such complicated 3-D structures, and the challenge has been met. All the fractal designs are able to operate at the 2.4-GHz Bluetooth band, and the final design (dual inverse fractal) covers both the 2.4- and 5-GHz WLAN bands. Previously proposed fractal designs required modification of the dimensions of the later iterations in order to achieve operation at the bands of existing wireless communication technologies [31]–[33]. In our case, the scale ratio between the repetitive patterns has been maintained and is the design that has evolved to improve input impedance at the higher band. The 3-D P technique employed is a binder jetting metal process. The technique is ideal for the highly detailed components of the fractals. Direct printing with metals rather than plating printed dielectrics is necessary to achieve adequate mechanical strength of these perforated structures (Fig. 1).

This paper is organized as follows. Section II describes the features that make this type of antenna suitable for 3-D P, introduces a novel dual fractal design, and discusses the fabrication and output features. Section III presents a novel design based on the inverse fractal antenna and analyzes its main characteristics. This paper finishes with a discussion and conclusion in Section IV. All antenna designs have been simulated using CST Microwave Studio and verified with experimental results.

II. 3-D Dual Fractal Antenna

A. Antenna Design and Analysis

The Sierpinski tetrahedral antenna [34], [35] is formed by removing scaled-down versions of an original solid tetrahedron in a repetitive process. This removal of material weakens the structure, so a procedure for providing adequate strength is outlined in this section. However, before this can be done, a brief outline of the design procedure follows. If the scale factor used is 0.5, each repetition results in four identical copies with their corners touching each other (Fig. 1). The number of tetrahedron created at the ith iteration is

$$N_i = 4^i. \tag{1}$$

All the sides of the tetrahedrons are equal in length, given by

$$L_i = \left(\frac{1}{2}\right)^i L_0 = 2^{-i} L_0 \tag{2}$$

where L_0 is the length of the side of the initial tetrahedron.

The height of each new tetrahedron, h_i, in relation to the total initial height H_0 and to the initial side L_0 is

$$h_i = \left(\frac{1}{2}\right)^i H_0 = \left(\frac{1}{2}\right)^i \sqrt{\frac{2}{3}} L_0. \tag{3}$$

In this fractal, the combined surface area of all faces of all tetrahedrons (both interior and exterior faces) is equal the total area of the original tetrahedron. If the total surface area of the original tetrahedron is A_0, the surface area of each tetrahedron created in iteration i is given by

$$A_i = \left(\frac{1}{4}\right)^i A_0. \tag{4}$$

The quantity A_i might be significant if not all faces were to be covered by depositing conducting material.

The total surface area at the ith iteration is then

$$A_{Ti} = 4^i \left(\frac{1}{4}\right)^i A_0 = A_0. \tag{5}$$

In general, the external faces are more important than the internal characteristics in antenna engineering. The total external surface area $A_{\mathrm{ET}i}$ is

$$A_{\mathrm{ET}i} = \left(\frac{3}{4}\right)^i A_0. \tag{6}$$

The reduction of the volume from the original nonfractal tetrahedron design (V_0) is an important factor when considering the cost of the material used for AM processes. The volume of each tetrahedron can be calculated as

$$V_i = \left(\frac{1}{8}\right)^i V_0. \tag{7}$$

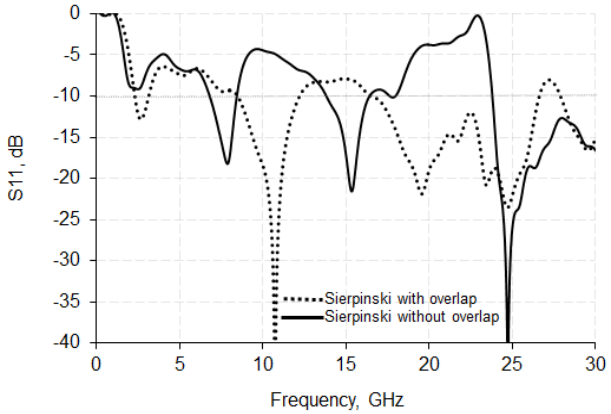

Fig. 2. Reflection coefficients of the Sierpinski fractal antenna with overlap and without overlap.

Thus, the total volume is given by

$$V_{Ti} = 4^i \left(\frac{1}{8}\right)^i V_0 = 2^{-i} V_0. \tag{8}$$

A 3-D Siepinski fractal antenna can be created by arranging the structure so that the feeding is connected to one of the vertices [35]. Three iterations have been applied in this illustration, giving a total number of 64 tetrahedrons. A Sierpinski antenna of total height H_0 of 22 mm was simulated, and its reflection coefficient (S_{11}) is presented in Fig. 2 as "without overlap." From (6) and (8), the designs use 42% of the external area and 12.5% of the volume and of the corresponding nonfractal tetrahedron. A circular metal ground plane with radius r of 70 mm was employed. In order to be able to fabricate the antenna using AM techniques and moreover to provide sufficient mechanical strength, every minor tetrahedron was overlapped with its neighbor. The overlap was 0.56 mm throughout. Fig. 1 illustrates the principle. This decreased the total height of the antenna from 22 to 18.1 mm. The modified design is presented as "with overlap" in Fig. 1(b); that is, successive tetrahedrons are merged into each other. The new design used 58% of the external area and 22% of the volume of an equivalent nonfractal tetrahedron of height 18.1 mm. The overlap increased the frequencies of most resonant modes and improved the S_{11} matching (Fig. 2). This design is able to operate at a 2.4-GHz band with further resonant modes at higher bands.

In order to improve the matching and better assess the manufacturing process, a new structure was created by adding a copy of the design and rotating by 60° around the z-axis. The resulting structure is shown in Fig. 3(b), and in Fig. 4, the feed arrangements are illustrated. This design uses 58% of the external area and just 22.4% of the volume of the equivalent nonfractal design. In order to provide mechanical strength, the inner cylinder of diameter of 2 mm from the coaxial input port was extended to the fractal antenna. The total height of 18 mm and the extent of the overlap were retained in the new design. The various distances of the repetitions to the metallic ground (Fig. 4) d_n (mm) can be calculated by the equation

$$d_n = 2d_{n-1} - 0.56 \tag{9}$$

where d_0 is 2.75 mm.

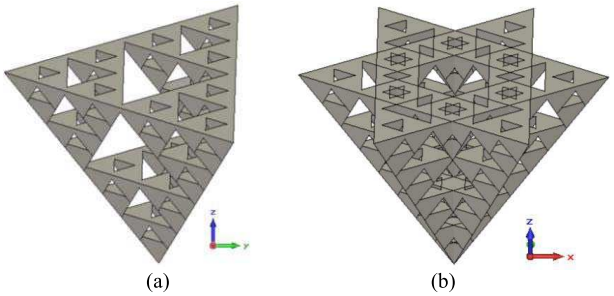

Fig. 3. Perspective view of (a) classical and (b) proposed fractal antennas.

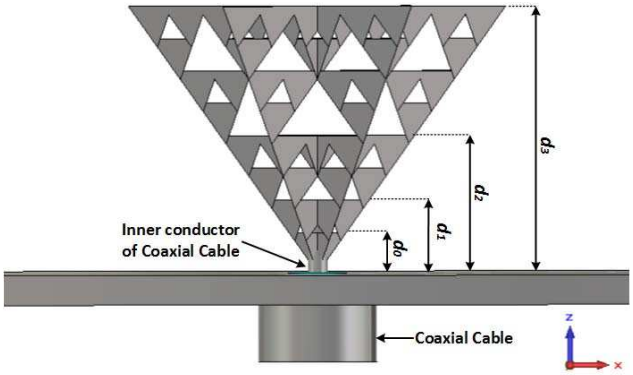

Fig. 4. Dual fractal design connected to the coaxial feedline and ground plane. The distances between repetitions n and the ground plane d_n are included.

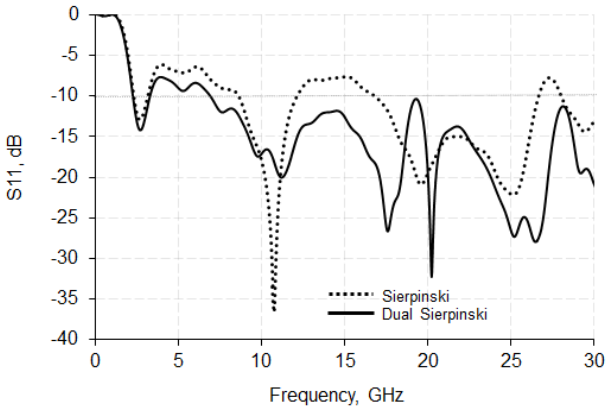

Fig. 5. Reflection coefficients of the initial Sierpinski [Fig. 2(b)] and new dual fractal (Fig. 4) antenna, both with overlap.

Fig. 5 shows the simulated S_{11} for the new antenna and its comparison with the initial Sierpinski design for a frequency range from 0 to 30 GHz. The new structure has further improved the impedance match, particularly at the higher bands. The −10-dB input match now covers from 6.9 to over 30 GHz. The first and second resonances are very similar in that both the initial fractal designs provide four bands, at 2.7, 10.8, 19.6, and 25.2 GHz. In contrast, the proposed dual fractal antenna has five different resonances, at 2.7, 11.2, 17.6, 20.2, and 25.2 GHz, in the same range.

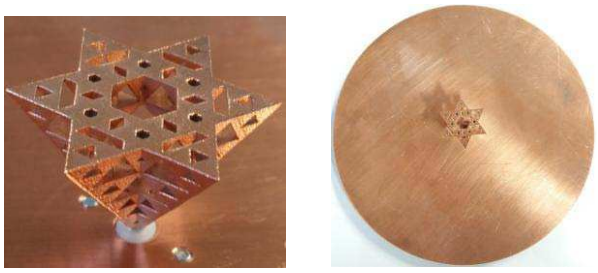

(a) (b)

Fig. 6. Photographs of the fabricated dual fractal antenna. (a) Oblique. (b) Top view.

B. Fabrication and Measurement

The complexity of the internal and external features of the new design makes it very difficult to fabricate using traditional subtractive techniques. In order to investigate the potential applicability of AM for 3-D fractal antenna development, a metal powder bed fusion process, and more specifically metal powder embinder printing, was employed [36], [37]. This metal technique was selected because of the mechanical robustness of the output and the possibility of printing highly detailed features. The technology prints the models by binding together layers of ultrafine grains of stainless steel powder in a precision inkjet printer. Once the printing is done, the part is sintered in an oven at 1300 °C. The design specifications required a minimum thickness wall of 0.3 mm and a minimum detail of 0.1 mm.

The digital model was exported from CST Microwave Studio to an STL format and then uploaded to the 3-D printer. AM using copper was unavailable. The base metal used was 316L stainless steel, a material with inferior conductivity. Consequently, a copper layer of approximately 50 μm was deposited on the antenna using an electroplating process readily available in the authors' laboratory at the University of Kent. This increased the surface conductivity of the copper layer. An aperture diameter of 2 mm was created during the design process, which was later used to feed the antenna with a 50-Ω SMA connector. Fig. 6 shows a photograph of a 3-D dual fractal antenna, consisting of a circular copper ground plane with a diameter of 140 mm and a thickness of 2 mm. The 3-D surface profiles of the fractal structure are shown in Fig. 7. The measured surface roughness was 1.92 μm (Sa), and the rms deviation of 2.46 μm (Sq).

The measured reflection coefficients of the dual fractal antenna are compared with simulations in Fig. 8. A Rohde & Schwarz ZVL vector network analyzer was used for the experiments. Good agreement was found between simulations and measurements. There was a slight increase in the resonant frequency and decrease in the input match at the first mode. However, the measured S_{11} was lower than those simulated at the higher bands. The differences between simulations and measurements are likely due to additive fabrication tolerances.

Radiation patterns were measured at various frequencies in an anechoic chamber. Fig. 9 shows the patterns in the *xy* and *xz* planes at 2.6, 5.5, and 11.5 GHz. The patterns were similar to those for a wideband monopole antenna on a large ground plane. They were omnidirectional in the *xy* plane with

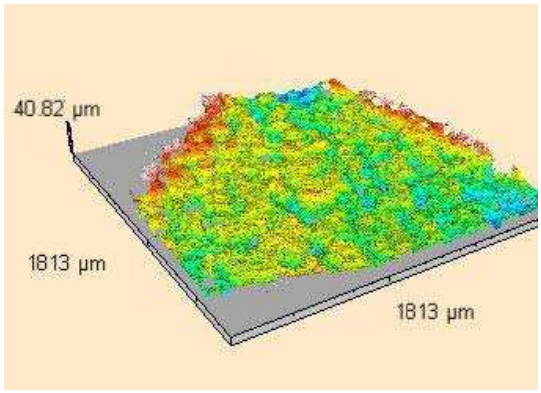

(a)

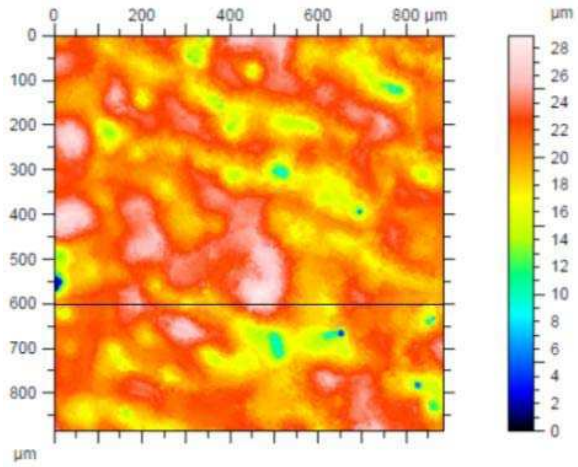

(b)

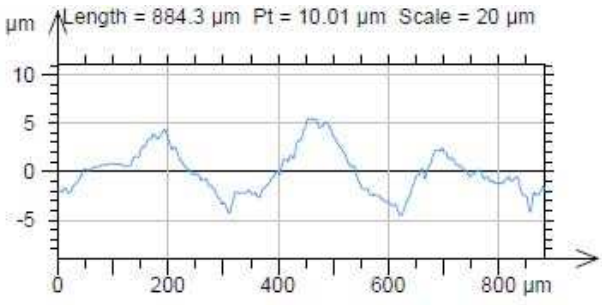

(c)

Fig. 7. Measured surface profile. (a) 3-D profile. (b) Zoomed-in view profile. (c) Profile 2-D cut.

a null in the *z*-axis. Low cross-polar levels were observed at the studied frequency bands, typically −20 dB or below. The computed gains were 3.91, 4.54, and 4.46 dB at 2.6, 5.5, and 11.5 GHz.

III. Fabrication of a 3-D Inverse Fractal Antenna

The 3-D fabrication of antennas based on the inverse fractal configuration [Fig. 10(c)] has also been studied. The geometry of the inverse Sierpinski fractal antenna has most of the complex features in the external faces, and therefore, its input matching is more likely to be sensitive to fabrication errors. This can provide a further assessment of the fabrication process. The antenna is developed as illustrated in Fig. 10.

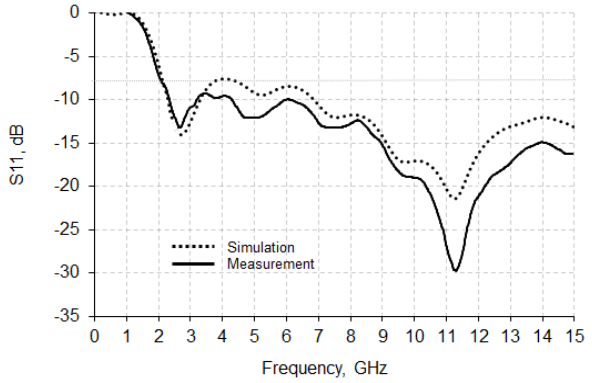

Fig. 8. Reflection coefficient of the dual fractal antenna.

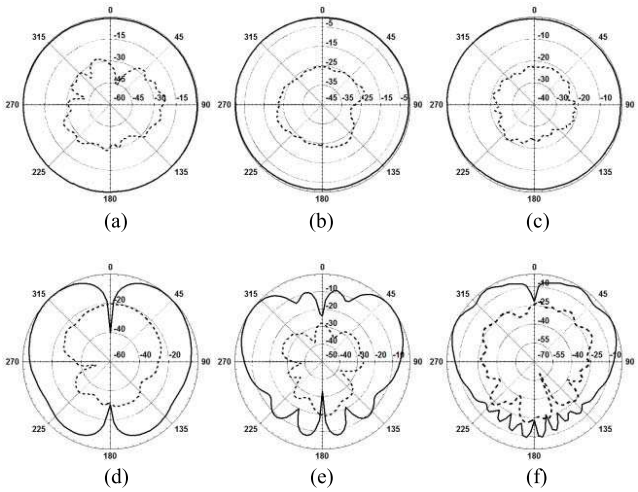

Fig. 9. Measured radiation pattern characteristic of the dual fractal antenna at various frequencies. (a) 2.6 GHz (*xy* plane). (b) 5.5 GHz (*xy* plane). (c) 11.5 GHz (*xy* plane). (d) 2.6 GHz (*xz* plane). (e) 5.5 GHz (*xz* plane). (f) 11.5 GHz (*xz* plane). Solid curves: co-polar and dotted curves: cross-polar.

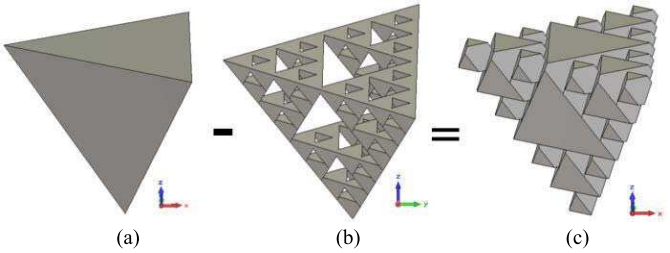

Fig. 10. Design process for inverse fractal antenna. (a) Tetrahedron. (b) Sierpinski fractal. (c) Inverse Sierpinski fractal.

Basically, the fractal design [Fig. 10(b)] is subtracted from a nonfractal tetrahedron [Fig. 10(a)], resulting in the structure in Fig. 10(c). As a complement of the original designs, the new structure occupies about 77% of the volume of the equivalent tetrahedron.

Simulations of this new configuration [Fig. 10(c)] resulted in the first resonant frequency of about 3 GHz. As the main aim of this paper was to construct antennas suitable for existing wireless systems, the dimensions were scaled by a factor of 1.27 in all directions. The height of the new design was 23 mm. The same technique used to develop the dual fractal antenna in Section II was then applied, resulting in

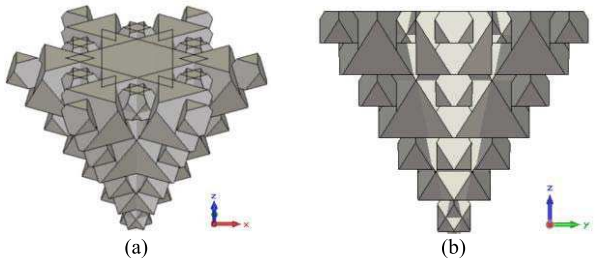

Fig. 11. Inverse dual fractal antenna. (a) Perspective view. (b) Side view.

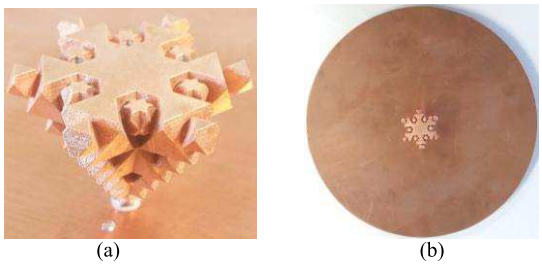

Fig. 12. Photographs of the fabricated of dual fractal antenna. (a) Oblique. (b) Top view.

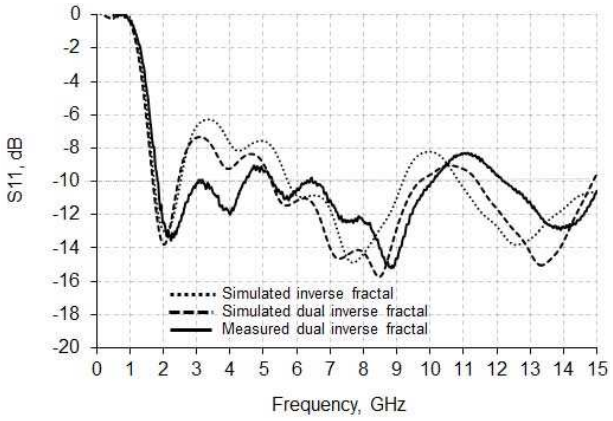

Fig. 13. Reflection coefficients of the inverse dual fractal antenna (Fig. 11) and the inverse fractal [Fig. 10(c)].

the configuration in Fig. 11. Again, a copy of the structure was rotated by 60° about the z-axis and then merged with the original design.

This antenna was fabricated by AM using the same procedure described earlier. The feeding of the antenna was again via a 50-Ω SMA connector through the center of the ground plane, as shown in Fig. 12.

The simulated and measured S_{11} of the dual inverse antenna, together with the simulated results for the initial inverse antenna [Fig. 10(c)], are shown in Fig. 13. The dual inverse fractal has improved impedance match. Both simulated and measured results are in good agreement. In the measurement, the resonant modes have shifted up by about 8% from the simulations. At the 2.4- and 5.5-GHz WLAN bands, and up to about 10 GHz, the S_{11} levels are -10 dB or below. The surface current distributions of the dual inverse fractal antenna for three resonant frequencies are shown in Fig. 14. As expected, the surface currents are spread over a larger area at lower frequencies. Little current is found at the top of the structure,

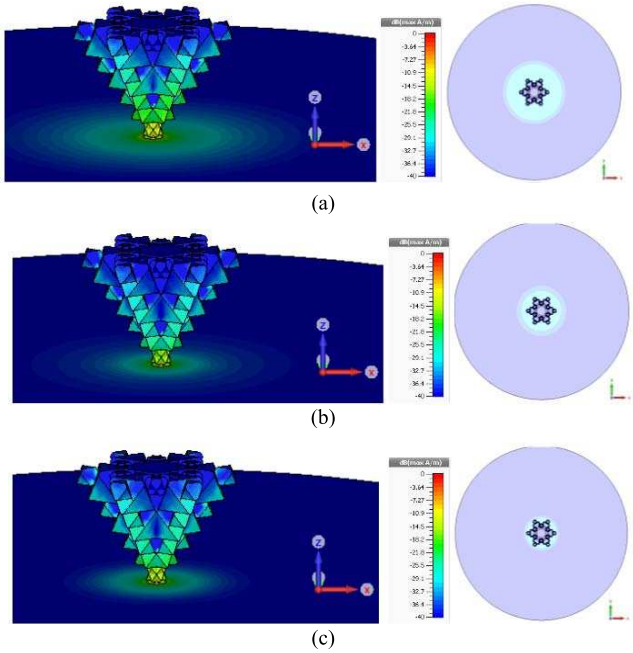

Fig. 14. Surface current density of the dual inverse fractal antenna at the frequencies. (a) 2.4 GHz. (b) 5.5 GHz. (c) 8 GHz.

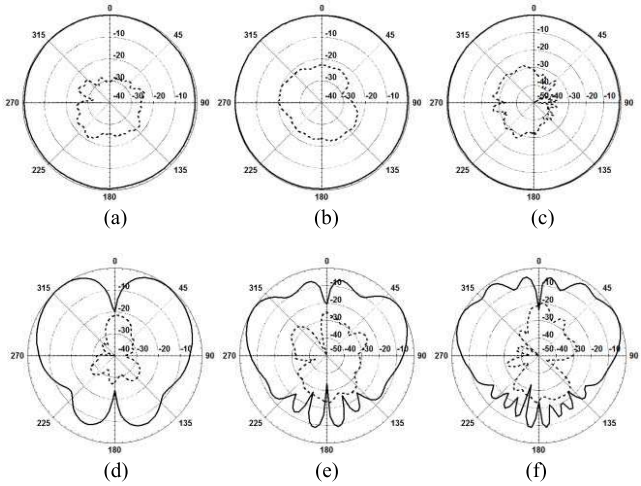

Fig. 15. Measured radiation pattern characteristic of the dual inverse Sierpinski fractal antenna (Fig. 11). (a) 2.4 GHz (*xy* plane). (b) 5.5 GHz (*xy* plane). (c) 8 GHz (*xy* plane). (d) 2.4 GHz (*xz* plane). (e) 5.5 GHz (*xz* plane). (f) 8 GHz (*xz* plane).

particularly at its center. This could be an indication that some of the materials could be removed, reducing the content below the 77% of the equivalent dual tetrahedron, without affecting the performance significantly.

The main sections of the measured radiation patterns of the dual inverse fractal design (Fig. 11) at three resonant frequencies of 2.4, 5.5, and 8 GHz are presented in Fig. 15. The patterns are mainly omnidirectional in the *xy* plane. For comparison, the patterns for the initial inverse fractal design [Fig. 10(c)] are presented in Fig. 16, and the patterns for the dual inverse fractal design are more omnidirectional and with lower cross-polar levels than those for the initial inverse fractal design.

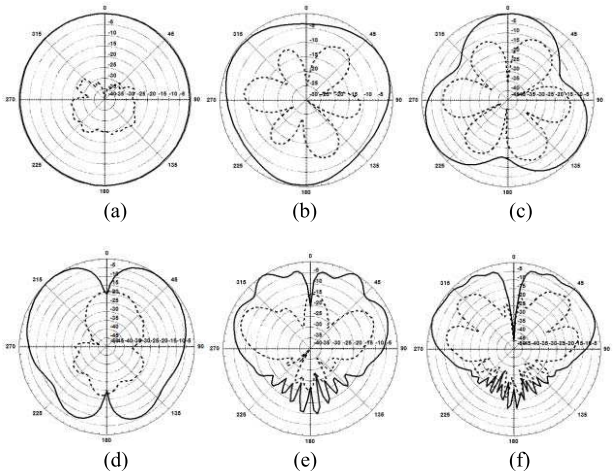

Fig. 16. Measured radiation pattern characteristic of the inverse fractal antenna [Fig. 10(c)] at the frequencies. (a) 2.4 GHz (*xy* plane). (b) 8.9 GHz (*xy* plane). (c) 13.8 GHz (*xy* plane). (d) 2.4 GHz (*xz* plane). (b) 8.9 GHz (*xz* plane). (c) 13.8 GHz (*xz* plane).

IV. Discussion and Conclusion

AM has been proven to be suitable for the development and fabrication of 3-D fractal antennas. The 3-D P with metals gives mechanical strength, particularly in the joints between the various repetitions of the fractal elements. The antennas can be fabricated using metal powder embinder printing and an additional electroplating process. The alternative option of plating printed dielectrics would have mechanical weakness at the joints. The structures presented here offer attractive electromagnetic features, and are also able to reduce the amount of material use in AM processes. A new dual fractal Siperpinski design improves antenna matching at higher bands compared with the original Sierpinski tetrahedron. More importantly, it decreases a volume usage by over 75% compared with the equivalent nonfractal design. The study included here indicates that significant material reduction can be achieved using Sierpinski fractals or similar structures, potentially reducing costs of manufacturing.

The inverse Sierpinski tetrahedron fractal has less smooth external features and therefore is more sensitive to fabrication processes. The imprecisions in the fabrication process produce a shift in the resonant frequencies of about 8% at all bands. However, the final dual inverse fractal design is still able to resonate at the 2.4- and 5.5-GHz WLAN bands, while also providing operational capability at higher frequencies, both in simulation and measurements. It also offers good omnidirectional pattern and low cross-polarization levels. The dual inverse fractal design uses 23% less material than the equivalent nonfractal design. Moreover, current flow simulations indicate that there is potential to reduce the amount of material further without affecting electrical performance.

There are very slight differences between simulations and measurements that probably arose from fabrication inaccuracies. Nevertheless, this paper demonstrates that this 3-D P technique is a relatively accurate and reliable method for fabricating complex radiating structures required to operate at frequencies below 15 GHz.

Fractal and complex antennas fabricated using 3-D P with metals have applications in the defense and aerospace sectors

where robustness as well as lightweight are key. The antennas could be integrated with other additive manufactured parts. For example, the present structure is less than 2 cm in height, but for operational at longer wavelengths or structures with higher iterations, a nonconducting dielectric support could be formed integrally with the antenna.

ACKNOWLEDGMENT

The authors would like to thank S. Jakes and Materialise NV for assisting in the fabrication of the antennas.

REFERENCES

[1] E. MacDonald *et al.*, "3D printing for the rapid prototyping of structural electronics," *IEEE Access*, vol. 2, pp. 234–242, 2014.

[2] T. P. Ketterl *et al.*, "A 2.45 GHz phased array antenna unit cell fabricated using 3-D multi-layer direct digital manufacturing," *IEEE Trans. Microw. Theory Techn.*, vol. 63, no. 12, pp. 4382–4394, Dec. 2015.

[3] A. Cloonan, D. Shahmirzadi, R. Li, B. Doyle, E. Konofagou, and T. McGloughlin, "3D-printed tissue-mimicking phantoms for medical imaging and computational validation applications," *3D Printing Additive Manuf.*, vol. 1, no. 1, pp. 14–23, 2014.

[4] M. Liang, C. Shemelya, E. MacDonald, R. Wicker, and H. Xin, "3-D printed microwave patch antenna via fused deposition method and ultrasonic wire mesh embedding technique," *IEEE Antennas Wireless Propag. Lett.*, vol. 14, pp. 1346–1349, 2015.

[5] H. Sigmarsson, E. Kinzel, X. Xu, and W. Chappell, "Selective laser sintering of multilayer, multimaterial circuit components," in *IEEE MTT-S Int. Microw. Symp. Dig.*, Jun. 2006, pp. 1788–1791.

[6] J. A. Lorente, M. M. Mendoza, A. Z. Petersson, L. Pambaguian, A. Melcon, and C. Ernst, "Single part microwave filters made from selective laser melting," in *Proc. Eur. Microw. Conf. (EuMC)*, Sep. 2009, pp. 1421–1424.

[7] C. R. Garcia, R. C. Rumpf, H. H. Tsang, and J. H. Barton, "Effects of extreme surface roughness on 3D printed horn antenna," *Electron. Lett.*, vol. 49, no. 12, pp. 734–736, Jun. 2013.

[8] M. D'Auria *et al.*, "3-D printed metal-pipe rectangular waveguides," *IEEE Trans. Compon., Packag., Manuf. Technol.*, vol. 5, no. 9, pp. 1339–1349, Sep. 2015.

[9] P. Nayeri *et al.*, "3D printed dielectric reflectarrays: Low-cost high-gain antennas at sub-millimeter waves," *IEEE Trans. Antennas Propag.*, vol. 62, no. 4, pp. 2000–2008, Apr. 2014.

[10] S. Zhang, "Design and fabrication of 3D-printed planar Fresnel zone plate lens," *Electron. Lett.*, vol. 52, no. 10, pp. 833–835, 2016.

[11] B. Sanz-Izquierdo and E. A. Parker, "3-D printing of elements in frequency selective arrays," *IEEE Trans. Antennas Propag.*, vol. 62, no. 12, pp. 6060–6066, Dec. 2014.

[12] B. Sanz-Izquierdo and E. A. Parker, "Frequency selective surfaces formed by partially metalising 3D printed shapes," in *Proc. 9th Eur. Conf. Antennas Propag. (EuCAP)*, 2015, pp. 1–4.

[13] S. Jun, B. Sanz-Izquierdo, and E. A. Parker, "3D printing technique for the development of non-planar electromagnetic bandgap structures for antenna applications," *Electron. Lett.*, vol. 52, no. 3, pp. 175–176, 2016.

[14] J. J. Adams *et al.*, "Conformal printing of electrically small antennas on three-dimensional surfaces," *Adv. Mater.*, vol. 23, no. 11, pp. 1335–1340, Mar. 2011.

[15] O. S. Kim, "Rapid prototyping of electrically small spherical wire antennas," *IEEE Trans. Antennas Propag.*, vol. 62, no. 7, pp. 3839–3842, Jul. 2014.

[16] A. G. López, E. E. C. López, R. Chandra, and A. J. Johansson, "Optimization and fabrication by 3D printing of a volcano smoke antenna for UWB applications," in *Proc. 7th Eur. Conf. Antennas Propag. (EuCAP)*, 2013, pp. 1471–1473.

[17] E. A. Parker and A. N. A. El Sheikh, "Convoluted array elements and reduced size unit cells for frequency-selective surfaces," *IEE Proc. H, Microw. Antennas Propag.*, vol. 138, no. 1, p. 19, 1991.

[18] C. Puente, J. Romeu, R. Pous, X. Garcia, and F. Benitez, "Fractal multiband antenna based on the Sierpinski gasket," *Electron. Lett.*, vol. 32, no. 1, p. 1, 1996.

[19] D. H. Werner and S. Ganguly, "An overview of fractal antenna engineering research," *IEEE Antennas Propag. Mag.*, vol. 45, no. 1, pp. 38–57, Feb. 2003.

[20] K. J. Vinoy, J. K. Abraham, and V. K. Varadan, "On the relationship between fractal dimension and the performance of multi-resonant dipole antennas using Koch curves," *IEEE Trans. Antennas Propag.*, vol. 51, no. 9, pp. 2296–2303, Sep. 2003.

[21] L. Lizzi and A. Massa, "Dual-band printed fractal monopole antenna for LTE applications," *IEEE Antennas Wireless Propag. Lett.*, vol. 10, pp. 760–763, 2011.

[22] K. C. Hwang, "Dual-wideband monopole antenna using a modified half-Sierpinski fractal gasket," *Electron. Lett.*, vol. 45, no. 10, p. 487, 2009.

[23] H. Oraizi and S. Hedayati, "Miniaturized UWB monopole microstrip antenna design by the combination of Giusepe Peano and Sierpinski carpet fractals," *IEEE Antennas Wireless Propag. Lett.*, vol. 10, pp. 67–70, 2011.

[24] V. V. Reddy and N. V. S. N. Sarma, "Compact circularly polarized asymmetrical fractal boundary microstrip antenna for wireless applications," *IEEE Antennas Wireless Propag. Lett.*, vol. 13, pp. 118–121, 2014.

[25] J. Romeu and Y. Rahmat-Samii, "Fractal FSS: A novel dual-band frequency selective surface," *IEEE Trans. Antennas Propag.*, vol. 48, no. 7, pp. 1097–1105, Jul. 2000.

[26] B. Sanz-Izquierdo, E. A. Parker, J. B. Robertson, and J. C. Batchelor, "Singly and dual polarized convoluted frequency selective structures," *IEEE Trans. Antennas Propag.*, vol. 58, no. 3, pp. 690–696, Mar. 2010.

[27] X. L. Bao, G. Ruvio, M. J. Ammann, and M. John, "A novel GPS patch antenna on a fractal Hi-impedance surface substrate," *IEEE Antennas Wireless Propag. Lett.*, vol. 5, no. 1, pp. 323–326, 2006.

[28] Y. Rahmat-Samii and H. Mosallaei, "Electromagnetic band-gap structures: Classification, characterization, and applications," in *Proc. 11th Int. Conf. Antennas Propag. (ICAP)*, 2001, pp. 560–564.

[29] J. S. Petko and D. H. Werner, "Miniature reconfigurable three-dimensional fractal tree antennas," *IEEE Trans. Antennas Propag.*, vol. 52, no. 8, pp. 1945–1956, Aug. 2004.

[30] H. Rmili, O. Mrabet, J.-M. Floch, and J.-L. Miane, "Study of an electrochemically-deposited 3-D random fractal tree-monopole antenna," *IEEE Trans. Antennas Propag.*, vol. 55, no. 4, pp. 1045–1050, Apr. 2007.

[31] R. Aziz, M. Alkanhal, and A. Sheta, "Multiband fractal-like antennas," *Prog. Electromagn. Res. B*, vol. 29, pp. 339–354, 2011.

[32] S. Rai, Y. Choukiker, and S. Behera, "Irregular circular fractal slot antenna for dual wideband applications," in *Proc. Int. Symp. Devices MEMS, Intell. Syst. Commun. (ISDMISC)*, 2011, pp. 1–4.

[33] R. Liu and W. He, "A novel Sierpinski fractal antenna for wireless application," in *Proc. 5th Int. Conf. Comput. Inform. Sci.*, Jun. 2013, pp. 1347–1348.

[34] C. Puente-Baliarda, J. Romeu, R. Pous, and A. Cardama, "On the behavior of the Sierpinski multiband fractal antenna," *IEEE Trans. Antennas Propag.*, vol. 46, no. 4, pp. 517–524, Apr. 1998.

[35] A. N. Jabbar, "Studying the effect of building block shape on Sierpinski tetrahedron fractal antenna behavior using FDTD-equivalent electric circuits," *J. Microw. Optoelectron. Electromagn. Appl.*, vol. 11, pp. 162–173, Apr. 2012.

[36] I. Gibson, D. Rosen, and B. Stucker, *Additive Manufacturing Technologies*, 1st ed. New York, NY, USA: Springer, 2015.

[37] H. Chen and Y. Zhao, "Process parameters optimization for improving surface quality and manufacturing accuracy of binder jetting additive manufacturing process," *Rapid Prototyping J.*, vol. 22, no. 3, pp. 527–538, 2016.

Sung Yun Jun received the M.S. degree in electrical engineering from Syracuse University, Syracuse, NY, USA. He has been pursuing the Ph.D. degree in electronic engineering with the University of Kent, Canterbury, U.K., since 2014.

His current research interests include wearable antennas, electromagnetic bandgap structures, ultra-wideband antennas, and 3-D printed antennas.

Benito Sanz-Izquierdo received the B.Sc. degree from the University of Las Palmas de Gran Canaria, Las Palmas, Spain, and the M.Sc. and Ph.D. degrees from the University of Kent, Canterbury, U.K., in 2002 and 2007, respectively.

From 2003 to 2012, he was a Research Associate with the School of Engineering and Digital Arts, University of Kent, and became a Lecturer of electronic systems in 2013. In 2012, he joined Harada Industries Ltd., U.K., where he developed novel antennas for the automotive industry. His current research interests include multiband antennas, wearable microwave devices, substrate-integrated waveguides components, electromagnetic bandgap structures, and frequency selective surfaces.

Edward (Ted) A. Parker received the M.A. degree in physics and the Ph.D. degree in radio astronomy from St. Catharine's College, Cambridge University, Cambridge, U.K.

He joined the University of Kent, Canterbury, U.K., in 1977, as a Reader, has been a Professor of radio communications since 1987, and is currently a Professor Emeritus. He established the Antennas Group, Electronics Laboratory, University of Kent. He is a member of the Livery of the Worshipful Company of Scientific Instrument Makers, London, U.K. His current research interests include the application of frequency selective surfaces, and the study and overhaul of antique clocks.

Prof. Parker is a member of the Institution of Engineering and Technology.

David Bird, photograph and biography not available at the time of publication.

Alan McClelland, photograph and biography not available at the time of publication.